

Collider Phenomenology for models of extra dimensions *

Kingman Cheung[†]

National Center for Theoretical Sciences, National Tsing Hua University, Hsinchu, Taiwan, R.O.C.

(Dated: November 21, 2018)

In this talk, we summarize the collider phenomenology and recent experimental results for various models of extra dimensions, including the large extra dimensions (ADD model), warped extra dimensions (Randall-Sundrum model), TeV^{-1} -sized extra dimensions with gauge bosons in the bulk, universal extra dimensions, and an 5D $\text{SU}(5)$ SUSY GUT model in AdS space.

I. INTRODUCTION

The standard model (SM) of particle physics can be considered the most successful model among various standard models (other standard models, e.g., the standard model of the sun and the standard model of cosmology are gaining ground as more and more data are available to refine the models. From now on the standard model is referred to the standard model of particle physics.) It has enjoyed great health for more than 30 years. The precision measurements at LEP have tested the SM to the level of 10^{-3} [1]. In addition, the last piece of quarks, the top quark, was found [2]. Nevertheless, as a theorist we believe the SM cannot be a final theory, because of the followings. (i) The SM has many parameters, most of which are the fermion masses. This is related to the flavor problem. In the SM, we have three generations of fermions, each of which seems to be a repetition of each other. We do not fully understand why it is so and why there are only three generations, not to mention the generation of the fermion mass pattern. (ii) The SM is not a real unification of all forces. It would be nice to embed the SM into a grand unification theory. (iii) The hierarchy problem tells us that the apparently only two scales in particle physics, the electroweak and Planck scales, are 16 – 17 orders of magnitude different, which gives an enormously large loop correction to the scalar boson mass. It requires a very precisely fine-tuned bare mass to cancel the loop correction in order to give a scalar boson mass of order $O(100)$ GeV. All these problems lead us to believe that there should be new physics beyond the SM. Most of us believe that the new physics should come in in the TeV scale. There is a hope that the upcoming LHC is the place for the next big discovery.

There are other observations that tell us that the SM is not satisfactory. The most striking evidence is the definite (though small) neutrino masses that are required in the neutrino oscillations. There are mounting evidences for the solar and atmospheric neutrino flux deficits that are best explained by neutrino oscillations. Most of us

also believe that there should be dark matter that fills up a substantial fraction of the universe. More surprisingly, there is another very mysterious component of the universe, which is revealed by recent balloon, supernova, and satellite experiments. It is clear that the SM cannot provide these components of the universe. In addition, the SM cannot fulfill all the requirements to give a sufficiently large enough baryon asymmetry of the universe.

The hierarchy problem has motivated a number of models beyond the SM. In recent years, a number of models in extra dimensions have been proposed. They provide an alternative view of the hierarchy problem into a geometric stabilization of the extra dimensions. But why do we believe there are extra dimensions? Well, many string theorists and mathematicians believe so.¹ If there exist extra dimensions, why do we not see them? One simple reason is that they are probably too small. Figure 1 illustrating this simple reason why we do not see the extra dimensions. The word “Physics” is sitting on the cylinder (extra dimensions), but when we see it from very far away, the cylinder is too small to be noticed.

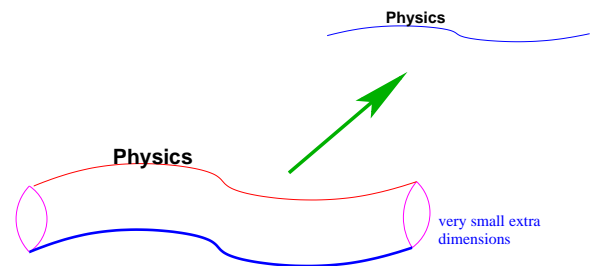


FIG. 1: Figure illustrating why we do not see the extra dimensions.

The main purpose of this talk is to review the collider phenomenology associated with extra dimension models, both theoretical and experimental works. Subsequent sections are devoted to various models, namely, (i) the large extra dimension model (ADD model), (ii) the warped extra dimension model (Randall-Sundrum mode), (iii) TeV^{-1} -sized model with gauge bosons in the

*The summary for a talk given at the invited session of “Beyond the Standard Model” in the APS/DPF April meeting, Philadelphia PA, U.S.A., April 2003. The talk is available at <http://nctsv06.phys.nthu.edu.tw/~cheung/extra-dim.pdf>

[†]Email: cheung@phys.cts.nthu.edu.tw

¹ I found an interesting cartoon to illustrate this point, but for the legal right reason I do not think I can put it here. It is at <http://www.th.physik.uni-frankfurt.de/~jr/gif/cartoon/cart0785.gif>

bulk, (iv) universal extra dimension model, and (v) an 5D SU(5) SUSY GUT model on a slice of AdS space.

II. ADD MODEL

It was proposed by Arkani, Dimopoulos, and Dvali [3] that the size R of the extra dimensions that only gravity can propagate can be as large as mm. This observation was based on the fact that no deviation from the Newton's law has been observed down to mm size. It has an important impact in our understanding of gravity. Suppose the fundamental Planck scale of the model is M_D , the observed Planck scale M_{Pl} becomes a derived quantity:

$$M_{Pl}^2 \sim M_D^{n+2} R^n,$$

where R is the size of the extra dimensions. This expression tells us that if R is extremely large, as large as a mm, the fundamental Planck scale M_D can be as low as TeV. Since the fundamental Planck scale is now at TeV, the hierarchy problem no longer exists. The setup is shown in Fig. 2. In this model, the SM particles and fields are confined to a brane while only gravity is allowed to propagate in the extra dimensions. Thus, the only probe of the extra dimensions must be through the graviton interactions, which is illustrated in Fig. 3. The graviton in the extra dimensions is equivalent to a tower of Kaluza-Klein (KK) states in the 4D point of view with a mass spectrum given by

$$M_l = \frac{l}{R},$$

where $l = 0, 1, 2, \dots$. The separation between each state is of order $1/R$, which is very small of order of $O(10^{-4})$ eV. This means that in the energy scale of current high energy experiments, the mass spectrum of the KK tower behaves like a continuous spectrum. Each of the KK states interacts with a strength of $1/M_{Pl}$ with the SM particles. However, when all the KK states are summed up, the interaction has a strength of $1/M_D$, where M_D is the real fundamental scale of the model and of order of $O(\text{TeV})$. Thus, we may be able to detect the graviton effects in current and future high energy experiments.

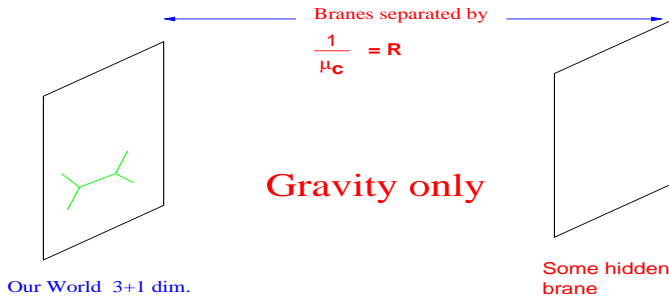


FIG. 2: The setup in the ADD model

The collider signatures for the ADD model can be divided into (i) sub-Planckian and (ii) trans-Planckian. From Fig. 3, it is clear that only graviton can probe the extra dimensions when the energy scale is below M_D . The SM particles scatter into a graviton, which can either (i) go into the extra dimensions and does not come back to the brane, which then gives rise to missing energy and momentum in experiments, or (ii) come back to the SM brane and decay back into SM particles, the scattering amplitude of which then interferes with the normal SM amplitude. Therefore, experimentally we can search for two types of signatures, the missing energy or the interference effects. When the energy scale is above the M_D , we expect the quantum gravity effects become important and objects, like black holes, string balls, p -branes would appear. In the following, we shall discuss these signatures one by one.

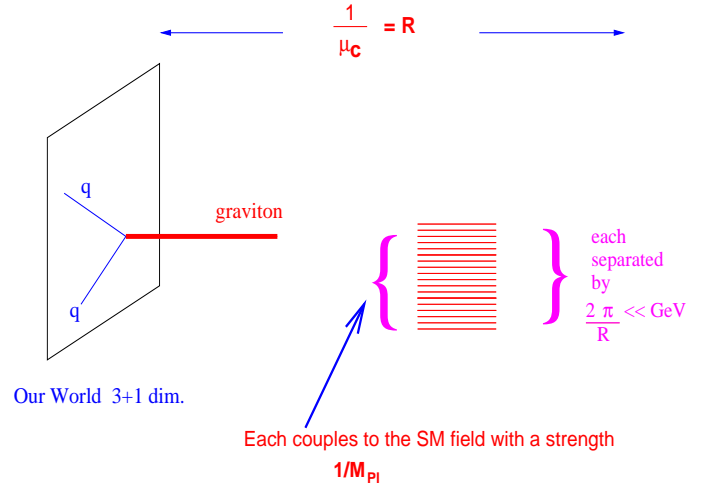


FIG. 3: The interactions of the graviton in the ADD model

A. Sub-Planckian

There have been enormous large amount of literature in this area [4, 5, 6, 7, 8, 9, 10, 11], so I only highlight on some of them and certainly show personal preference. As mentioned above the sub-Planckian signatures can be further categorized into those involving graviton emission and the virtual graviton exchanges. Let us first discuss the processes with graviton emission. The cleanest and easiest-to-see signature would be a single photon or a gauge boson with the missing energy due to the disappearance of the graviton into the extra dimensions [6, 10, 11]. The processes are

$$e^+e^- \rightarrow \gamma(Z)G$$

at e^+e^- colliders and

$$q\bar{q}(gg) \rightarrow gG$$

at hadronic colliders.

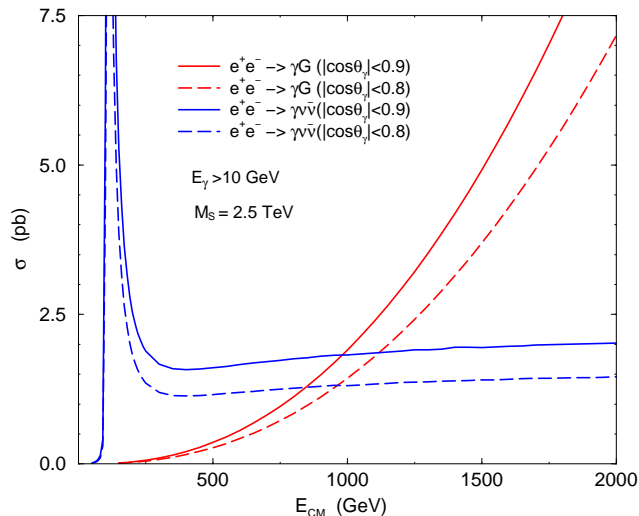


FIG. 4: Cross sections for $e^+e^- \rightarrow \gamma G$ compared with the SM background $e^+e^- \rightarrow \gamma \nu \bar{\nu}$. From Ref. [10].

In Fig. 4, we show the production cross section for $e^+e^- \rightarrow \gamma G$ vs the center-of-mass energy and compare with the SM background of $e^+e^- \rightarrow \gamma \nu \bar{\nu}$. The graviton signal easily surpasses the background at $\sqrt{s} \sim 0.8 - 1$ TeV for a $M_S = 2.5$ TeV.² Other related processes include $e^+e^- \rightarrow ZG$ and $e^+e^- \rightarrow f\bar{f}G$. The LEP collaborations have searched for these channels and obtained the limit on $M_D \sim 1$ TeV. The CDF collaboration also searched for events with a single photon plus missing energies, but no deviation is observed and they put a limit on $M_S > 0.55 - 0.6$ TeV for $n = 4 - 6$ [12]. The DØ collaboration searched for events of a single jet with missing energies. The limit they obtained is $0.89 - 0.62$ TeV for $n = 2 - 7$ [13].

For the processes involving virtual graviton exchanges the signatures would be the interference with the SM amplitudes, resulting in enhancement in the cross sections, especially at high energy [4, 5]. The signals that are easiest to detect are hadronic dilepton [7, 14, 15] and diphoton production [15, 16, 17], fermion-pair production at e^+e^- colliders [14, 18, 19]. Other avenues include gauge-boson pair production [20, 21, 22], dijet production [23], and top-quark production [24], as well as the anomalous muon magnetic moment [25].

Figure 5 illustrates the effect of graviton exchanges in the diphoton production at the Tevatron. Enhancement of the cross section can be seen at $M_{\gamma\gamma}$ much smaller than M_S . Therefore, the process can probe a fundamental Planck scale considerably higher than the energy of the collider. Another interesting process is the light-by-light

scattering [16]. The SM amplitude has to go through a box diagram while the graviton-induced amplitude is at tree-level. Thus, the effect of graviton exchanges is more conspicuous. Other processes that have been searched in experiments include $e^+e^- \rightarrow \gamma\gamma, WW, ZZ$ at LEP II (see the review in Ref. [69]), DIS scattering at HERA, as well as diphoton+dilepton production at the Tevatron by DØ. We are going to give more details on the last one, because it gives the best limit on M_S so far.

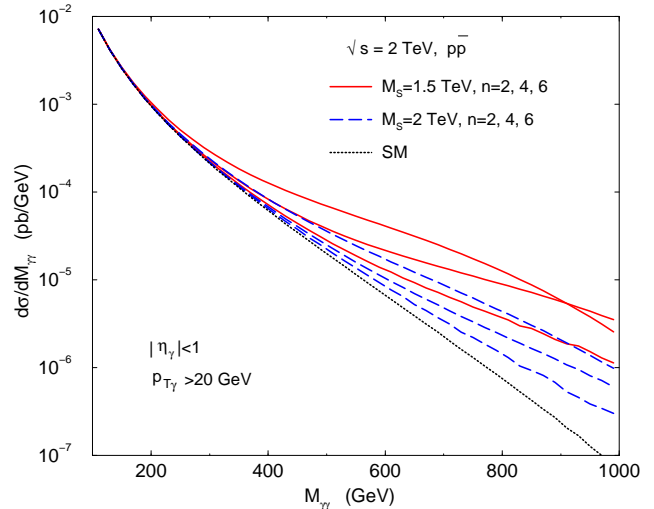


FIG. 5: The diphoton invariant mass spectrum for the process $p\bar{p} \rightarrow \gamma\gamma$ at the 2 TeV Tevatron. From Ref. [16].

Cheung and Landsberg [15] improved the previous analysis on diphoton and dilepton production using the 2D spectrum, $d^2\sigma/d\cos\theta^*dM$, where θ^* is the center-of-mass frame scattering angle and M is the invariant mass of the photon or lepton pair. The advantage of using a 2D spectrum is that for a $2 \rightarrow 2$ process two kinematical variables can cover all the phase space, therefore there is no need for cuts to optimize the effect. In Fig. 6, we show the 2D spectrum of the dilepton process. It is clear that the interference term and the pure graviton term are very different from the SM term. Moreover, a photon and an electron behave very similarly to each other in the detector. Therefore, instead of losing efficiency in identifying them, we can simply take both of them as events of electromagnetic showers. DØ [26] used this approach to search for the signal, but the data agreed well the SM and they placed limits on M_S . The limits are shown in Fig. 7. The limit is from 0.97 to 1.44 TeV for $n = 2 - 7$. So far, this is the best limit. We can also study the sensitivity reach on M_S in the future collider experiments at Tevatron Run II and at the LHC [15], which are shown in Table I.

² There are a few conventions of the fundamental scale in literature. They are related to each other through multiplicative constants. e.g., $M_D = [(2\pi)^n/(8\pi)]^{\frac{1}{n+2}} M_S$.

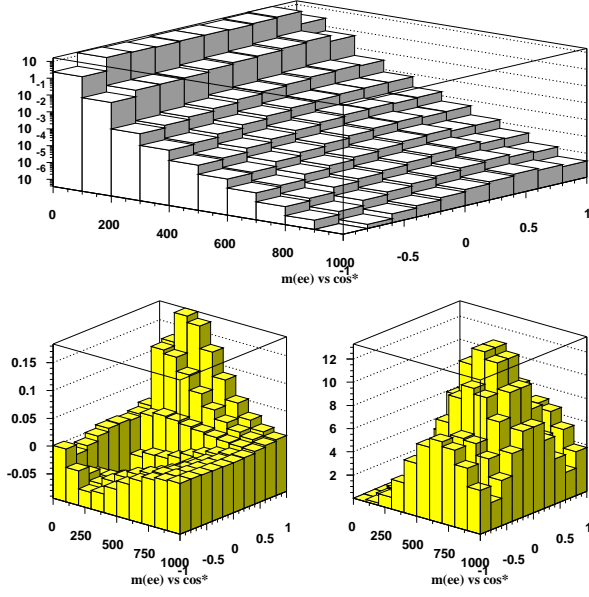


FIG. 6: The dilepton invariant mass spectrum for the process $p\bar{p} \rightarrow \ell^+\ell^-$ at the 2 TeV Tevatron. From Ref. [15].

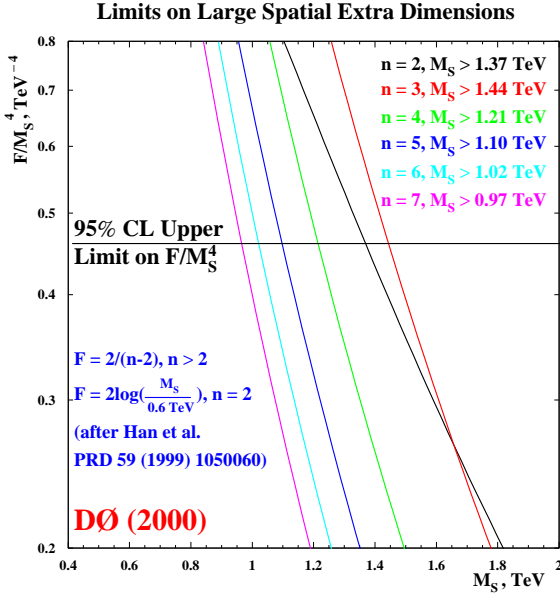


FIG. 7: The limits on M_S obtained by the DØ collaboration. This is taken from Ref. [26].

B. Trans-Planckian

Since the fundamental Planck scale is at TeV, so at the future hadronic collider, the LHC, the energy can surpass the fundamental Planck scale. Particle scattering would show the features of quantum gravity [27, 28, 29], be-

TABLE I: Sensitivity reach on M_S at Tevatron Run II and at the LHC.

	M_S (TeV)					
	$n = 2$	$n = 4$	$n = 6$	$n = 2$	$n = 4$	$n = 6$
Run I						
Dilepton	1.2	1.1	0.93			
Diphoton	1.4	1.2	1.0			
Combined	1.5	1.3	1.1			
Run IIa						
Dilepton	1.9	1.6	1.3	2.7	2.1	1.8
Diphoton	2.4	1.9	1.6	3.4	2.5	2.1
Combined	2.5	1.9	1.6	3.5	2.6	2.2
LHC						
Dilepton	10	8.2	6.9			
Diphoton	12	9.5	8.0			
Combined	13	9.9	8.3			

cause the fundamental Planck scale is at which the quantum gravity effects become strong. The cartoon in Fig. 8 shows the behavior of the scattering when the energy scale is getting higher and higher. When it approaches the string scale, the scattering is characterized by string scattering. As energy further increases, the string becomes highly excited and entangled like a string ball [30]. Eventually, the energy reaches a transition point and everything will turn into a black hole.

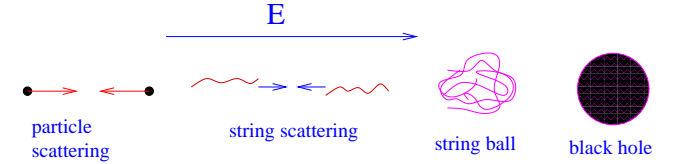


FIG. 8: Figure showing the trans-Planckian signatures.

A black hole (BH) is characterized by its mass, charge, and angular momentum. Here we simply look at the uncharged and nonrotating BH. The Schwarzschild radius and entropy of a BH with a mass M_{BH} in $n+4$ dimensions are given by, respectively, [31]

$$R_{\text{BH}} = \frac{1}{M_D} \left(\frac{M_{\text{BH}}}{M_D} \right)^{\frac{1}{n+1}} \left(\frac{2^n \pi^{\frac{n-3}{2}} \Gamma(\frac{n+3}{2})}{n+2} \right)^{\frac{1}{n+1}} \quad (1)$$

$$S_{\text{BH}} = \frac{4\pi}{n+2} \left(\frac{M_{\text{BH}}}{M_D} \right)^{\frac{n+2}{n+1}} \left(\frac{2^n \pi^{\frac{n-3}{2}} \Gamma(\frac{n+3}{2})}{n+2} \right)^{\frac{1}{n+1}} \quad (2)$$

As argued in a number of papers [32, 33], the entropy of the BH must be large in order that the object is in fact a BH. Here we follow the convention that the entropy $S_{\text{BH}} \gtrsim 25$. We show the entropy S_{BH} vs the mass of the BH in Fig. 9. It is clear that the entropy increases with

the mass, and the requirement of $S_{\text{BH}} \gtrsim 25$ is roughly equivalent to $M_{\text{BH}} > 5M_D$.

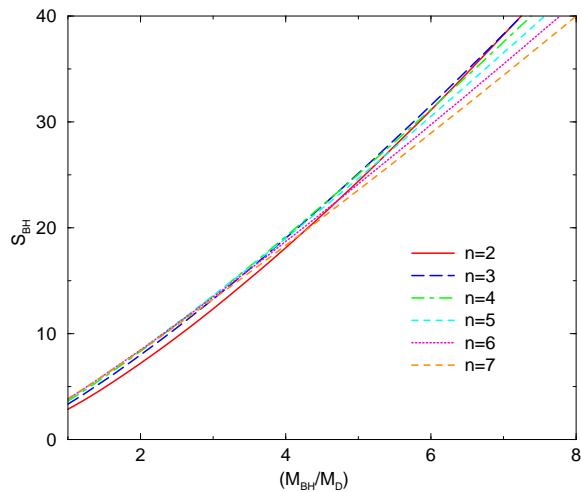


FIG. 9: Entropy of a BH vs its mass. From Ref. [36].

The production cross section of a BH in a collision is given by [28, 29]

$$\sigma = \pi R_{\text{BH}}^2, \quad (3)$$

which is based on a naive semi-classical argument. Suppose the two incoming particles involved in the collision have a center-of-mass energy \sqrt{s} and they want to coalesce into a BH, they can only do so if they are within the event horizon of the BH to be produced. Therefore, they can only produce a BH if their impact parameter is less than the radius, and thus resulting in the cross section formula above. The decay of the BH is somewhat complicated. Naively, one would expect the BH, as a quantum gravity object, would decay into gravitons, which then go to the extra dimensions and get lost. Experimentally, it would not be seen. However, the work by Emparan, Horowitz, and Myers [34] showed that it is not the case. Since the main phase of the BH decay is via the Hawking radiation, the wavelength corresponding to the Hawking temperature is much larger than the R_{BH} . Thus, the BH behaves like a s -wave point source and decays equally into the brane and bulk modes. Since in the setup there is only one graviton in the extra dimensions, but all SM particles on the brane, so the BH decays most of the time into the brane particles,³ i.e., the SM particles, and it could be observed in experiments. The BH decays “blindly” according to the particle degrees of freedom. The ratio

$$Z, W, H, \gamma, g; \quad u, d, s, c, b, t; \quad e, \mu, \tau, \nu_e, \nu_\mu, \nu_\tau = 30 : 72 : 18$$

and the ratio of hadronic:leptonic $\sim 5 : 1$. In addition, a nonrotating BH decays isothermally, and so for a BH of

a few TeV it decays into 30 – 50 particles, each of which then has an energy of a few hundred GeV. Therefore, the BH event will look like a spherical fireball [33, 36]. Such events are very clean and suffer from no background in collider experiments. One can do the event counting. We give the estimates for the BH production cross section at the LHC in Table II [33, 36].

TABLE II: Cross section in pb for BH production at the LHC. Here we included the contributions for the $2 \rightarrow 1$ and $2 \rightarrow 2$ subprocesses, and $y \equiv M_{\text{BH}}/M_D$.

	$n = 4$	$n = 5$	$n = 6$
$M_D = 1.5 \text{ TeV}$			
$y = 1$	9200	13000	18000
$y = 2$	890	1250	1600
$y = 3$	110	150	190
$y = 4$	12	15	21
$y = 5$	0.99	1.3	1.6
$M_D = 3 \text{ TeV}$			
$y = 1$	179	240	330
$y = 2$	2.3	3.2	4.3
$y = 3$	0.0085	0.011	0.015
$y = 4$	2.6×10^{-7}	3.5×10^{-7}	4.5×10^{-7}
$y = 5$	-	-	-

Other trans-Planckian objects include string balls [30] and p -branes [37]. Dimopoulos and Emparan [30] pointed out that when a BH reaches a minimum mass, it will transit into a state of highly excited and jagged strings – string balls (SB), the transition point is at

$$M_{\text{BH}}^{\text{min}} = M_s/g_s^2,$$

where M_s is the string scale and g_s is the string coupling. SBs can be considered the stringy progenitors of BHs. The correspondence principle states that the properties of a BH with a mass M_{BH} match those of a string ball of a string theory with $M_s/g_s^2 = M_{\text{BH}}$. Thus, their production cross section at the transition point should match, i.e.,

$$\sigma(\text{SB})|_{M_{\text{SB}}=M_s/g_s^2} = \sigma(\text{BH})|_{M_{\text{BH}}=M_s/g_s^2}. \quad (4)$$

We can parameterize the production cross section of the SB as follows. When the energy is above M_s but below M_s/g_s , the scattering is described by string-string scattering, the amplitude of which should scale as $\sim \hat{s}/M_s^4$. When the energy reaches M_s/g_s , saturation of unitarity sets σ to be a constant until it hits the correspondence point, after which the SB production cross section is replaced by the BH cross section. Thus, we have the following for the SB/BH production:

³ For alternative viewpoints on BH decays, see Refs. [35].

$$\hat{\sigma}(\text{SB/BH}) = \begin{cases} \frac{\pi}{M_D^2} \left(\frac{M_{\text{BH}}}{M_D} \right)^{\frac{2}{n+1}} [f(n)]^2 & \frac{M_s}{g_s^2} \leq M_{\text{BH}} \\ \frac{\pi}{M_D^2} \left(\frac{M_s/g_s^2}{M_D} \right)^{\frac{2}{n+1}} [f(n)]^2 = \frac{\pi}{M_s^2} [f(n)]^2 & \frac{M_s}{g_s^2} \leq M_{\text{SB}} \leq \frac{M_s}{g_s^2} \\ \frac{\pi g_s^2 M_{\text{SB}}^2}{M_s^4} [f(n)]^2 & M_s \ll M_{\text{SB}} \leq \frac{M_s}{g_s} \end{cases} \quad (5)$$

where

$$f(n) = \left(\frac{2^n \pi^{\frac{n-3}{2}} \Gamma(\frac{n+3}{2})}{n+2} \right)^{\frac{1}{n+1}}$$

The decay of a SB would be similar to the BH, and thus most of the time into the SM particles.

A p -brane is a solution to the Einstein equation in multi dimensions. A BH is considered a 0-brane, therefore p -branes, in principle, can also be produced in hadronic collisions. Consider an uncharged, static p -brane with mass $M_{p\text{B}}$. The p -brane wraps on $r(\leq m)$ small extra dimensions and on $p-r(\leq n-m)$ large extra dim. ⁴ The radius of the p -brane is given by

$$R_{p\text{B}} = \frac{1}{\sqrt{\pi M_*}} \gamma(n, p) V_{p\text{B}}^{\frac{1}{1+n-p}} \left(\frac{M_{p\text{B}}}{M_*} \right)^{\frac{1}{1+n-p}} \quad (6)$$

where

$$V_{p\text{B}} = l_{n-m}^{p-r} l_m^r \approx \left(\frac{M_{\text{Pl}}}{M_*} \right)^{\frac{2(p-r)}{n-m}},$$

$$\gamma(n, p) = \left[8\Gamma\left(\frac{3+n-p}{2}\right) \sqrt{\frac{1+p}{(n+2)(2+n-p)}} \right]^{\frac{1}{1+n-p}}.$$

Note that $R_{p\text{B}} \rightarrow R_{\text{BH}}$ in the limit $p = 0$. The production cross section of the p -brane is similar to the BH, given by

$$\hat{\sigma}(M_{p\text{B}}) = \pi R_{p\text{B}}^2. \quad (7)$$

The radius $R_{p\text{B}}$ of a p -brane is suppressed by some powers of the volume $V_{p\text{B}}$ wrapped by the p -brane. In order to achieve the maximum cross section, the value of $V_{p\text{B}}$ should be minimum, which occurs when the p -brane

wraps entirely on the small extra dimensions only, i.e., $r = p$. The ratio of p -brane cross section to BH cross section is given by

$$R \equiv \frac{\hat{\sigma}(M_{p\text{B}} = M)}{\hat{\sigma}(M_{\text{BH}} = M)} = \left(\frac{M_*}{M_{\text{Pl}}} \right)^{\frac{4(p-r)}{(n-m)(1+n-p)}} \left(\frac{M}{M_*} \right)^{\frac{2p}{(1+n)(1+n-p)}} \left(\frac{\gamma(n, p)}{\gamma(n, 0)} \right)^2 \quad (8)$$

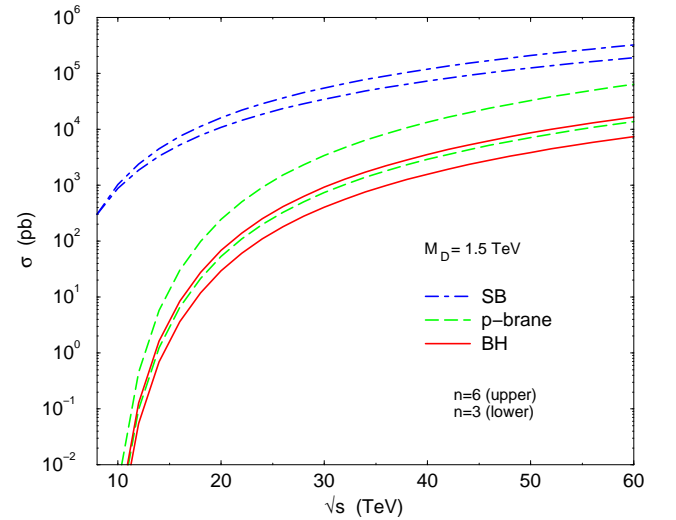


FIG. 10: Production cross sections for black holes, string balls, and p -branes. We have chosen $M_D = 1.5$ TeV, $M_{\text{BH}}^{\text{min}} = 5M_D$, and $M_{\text{SB}}^{\text{min}} = 2M_s$. From Ref. [36].

A comparison of production cross sections of BHs, SBs, and p -branes is shown in Fig. 10. Since the production threshold of SBs is much lower than BHs, SB cross section is therefore much larger. The p -brane cross section is somewhat larger than the BHs.

⁴ The configuration has n total extra dimensions, of which m dimensions are small ($\sim 1/M_*$) and $n-m$ are large ($\gg 1/M_*$). Here M_* is another notation in literature for the fundamental Planck scale, $M_* = M_S$.

Feng and Shapere [38] pointed out another possibility of observing the BH in the ultra-high energy cosmic ray (UHECR) experiments. The UHECR is the beam while our atmosphere is the target. The UHECR has a neutrino component that can penetrate deeply into the atmosphere without interacting. It is the neutrino component in the UHECR that produces the distinct signature for BHs. The largest chance that a neutrino can interact with the nucleons in the atmosphere to produce a BH is when it traverses horizontally across the atmosphere (shown in the cartoon of Fig. 11.) The BH then decays instantaneously, thus producing a horizontal air shower. Such deeply penetrating horizontal air showers are to be counted and compare with the SM prediction. The number of BH events expected for the run at the Pierre-Auger Observatory is shown in Fig. 12. A partial list of works in this area are listed in Refs. [39].

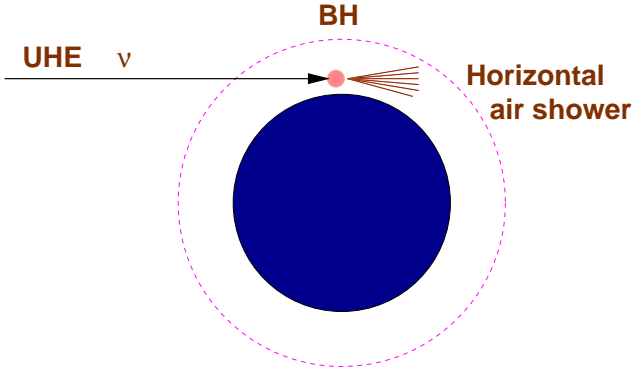


FIG. 11: Cartoon showing that the UHECR neutrino produces a BH and gives a horizontal air shower.

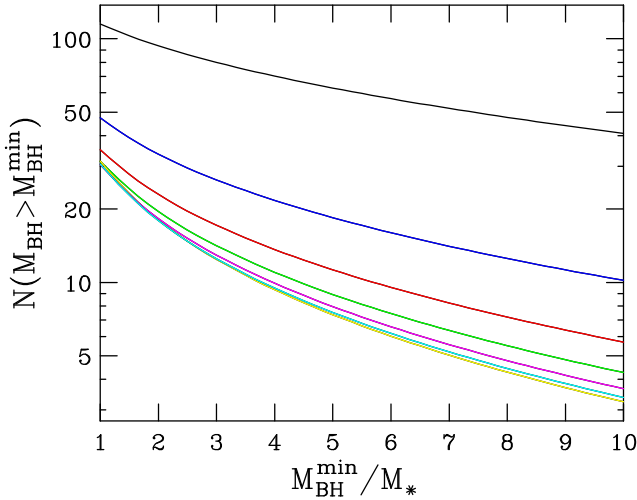


FIG. 12: Number of BH events detected by the ground array in 5 Auger site-years for $n = 1 - 7$ from above. This is taken from Ref. [38].

III. RANDALL-SUNDRUM MODEL

The Randall-Sundrum (RS) model [40] beautifully explains the gauge hierarchy with a moderate number through the exponential. The setup of the branes and the bulk is shown in Fig. 13.

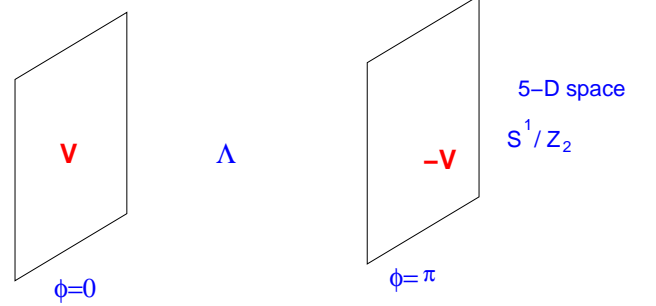


FIG. 13: The setup in the Randall-Sundrum model.

Just like the ADD model, since only graviton propagates in the extra dimensions, only gravity can probe the extra dimensions. However, the graviton KK states are very different from the ADD model. The most distinct feature of the RS model is the unevenly spaced KK spectrum for the gravitons, namely, proportional to the zeros of the n th modified Bessel function [41]. Phenomenology associated with the modulus field (known as the radion), describing the fluctuation in the separation of the two branes, is another interesting feature of the RS model [42, 43]. There is also the possibility that the radion can mix with the Higgs boson [44].

A. Graviton

The graviton field can be obtained by fluctuation of the metric

$$G_{\alpha\beta} = e^{-2ky} \eta_{\alpha\beta} + 2h_{\alpha\beta} / M_5^{3/2}. \quad (9)$$

After compactification, the KK states of the graviton has the spectrum given by

$$m_n = x_n \frac{\Lambda_\pi}{\sqrt{2}} \frac{k}{M_{\text{Pl}}} \quad (10)$$

where x_n is the zero of the n -th modified Bessel function. Numerically, $x_1, x_2, x_3 = 3.83, 7.02, 10.17$, respectively. Note that the spectrum is very different from that of flat metric. The interactions are given by

$$\mathcal{L} = -\frac{1}{M_{\text{Pl}}} T^{\mu\nu} h_{\mu\nu}^{(0)} - \frac{1}{\Lambda_\pi} T^{\mu\nu}(x) \sum_{n=1}^{\infty} h_{\mu\nu}^{(n)}(x), \quad (11)$$

from which we can see that the zeroth mode essentially decouples because the coupling is suppressed by $1/M_{\text{Pl}}$ while the KK states have a coupling strength of $1/\Lambda_\pi$.

The phenomenology of the RS model is very different from the ADD model in two aspects: (i) the spectrum of the graviton KK states are discrete and unevenly spaced while it is uniform, evenly spaced, and effectively a continuous spectrum in the ADD model, and (ii) each resonance in the RS model has a coupling strength of $1/\text{TeV}$ while in the ADD model only the collective strength of all graviton KK states gives a coupling strength of $1/\text{TeV}$.

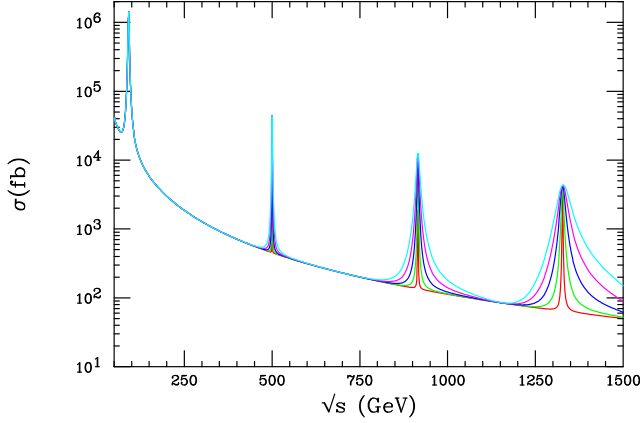


FIG. 14: Cross section of $e^+e^- \rightarrow \mu^+\mu^-$ vs \sqrt{s} , including the effects of the RS graviton KK states. This is taken from Ref. [66].

Figure 14 shows the resonance spectrum in the channel $e^+e^- \rightarrow \mu^+\mu^-$. The resonance spectrum clearly indicates that it is a discrete one and is unevenly spaced. The best present limit comes from the Drell-Yan production at the Tevatron. The effects of the graviton KK states on the Drell-Yan production at the Tevatron and at the LHC are summarized in Fig. 15. Davoudiasl et al. [41, 45] showed that the present Drell-Yan data can rule out a portion of the parameter space of the RS model. The constrained parameter space is shown in Fig. 16. The Tevatron Drell-Yan data ruled out a small portion of the parameter space to the left of the line. In addition, the constraints from oblique corrections also ruled out another portion of the parameter space to the lower of the line.⁵ Other constraints due to the naturalness of the model are also imposed. The sensitivity at the LHC (10 and 100 fb^{-1}) are also shown.

B. Radion

The RS model has a 4D massless scalar, radion, describing the fluctuation in the background metric

$$ds^2 = e^{-2k\phi T(x)} g_{\mu\nu}(x) dx^\mu dx^\nu - T^2(x) d\phi^2$$

⁵ According to a source, the calculation of the oblique correction might contain an error such that this line might not be correct.

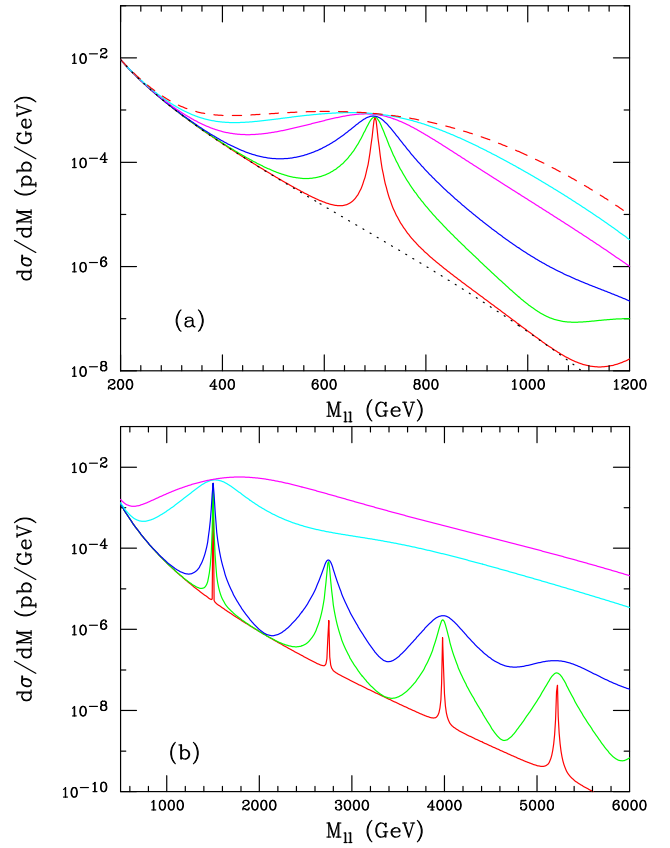


FIG. 15: The invariant mass distribution for the Drell-Yan process at the (a) Tevatron and (b) the LHC. This is taken from Ref. [45].

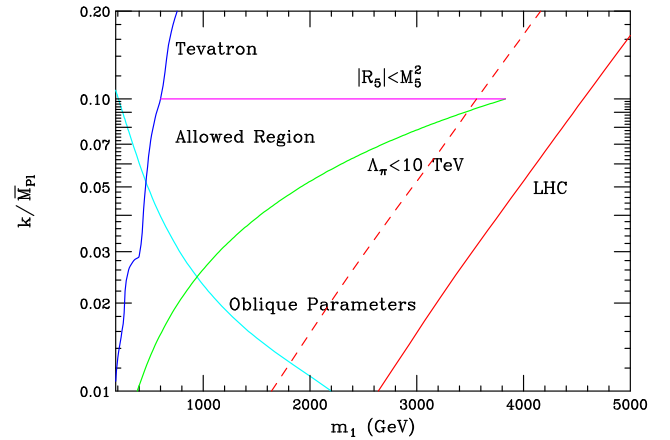


FIG. 16: The constrained parameter space of the RS model by the Drell-Yan process at the Tevatron and the oblique parameters. The constraints from the hierarchy of the RS model are also imposed. The sensitivity reach at the LHC are also shown. This is taken from Ref. [66].

where $T(x)$ is the modulus field (radion) describing the distance between the two branes. Since the gauge hierarchy is explained by a particular brane separation, a stabilization mechanism is necessary to achieve that.

Goldberger and Wise [42, 43] used a bulk scalar field to generate a potential, and the modulus field acquires a $O(0.1 - 1 \text{ TeV})$ mass with a coupling strength $1/\text{TeV}$.

The interactions of the radion with the SM particles are given by

$$\mathcal{L}_{\text{int}} = \frac{\phi}{\Lambda_\phi} T_\mu^\mu(\text{SM}), \quad (12)$$

where $\Lambda_\phi = \langle \phi \rangle$ is of order TeV and

$$T_\mu^\mu(\text{SM}) = \sum_f m_f \bar{f} f - 2m_W^2 W_\mu^+ W^{-\mu} - m_Z^2 Z_\mu Z^\mu + (2m_h^2 h^2 - \partial_\mu h \partial^\mu h) + \dots \quad (13)$$

It is clear that the interactions are very similar to those of the SM Higgs boson with the replacement of the vacuum expectation value. However, the radion has anomalous couplings from the trace anomaly to a pair of gluons (photons), in addition to the loop diagrams with the top-quark (the top-quark and W boson):

$$T_\mu^\mu(\text{SM})^{\text{anom}} = \sum_a \frac{\beta_a(g_a)}{2g_a} F_{\mu\nu}^a F^{a\mu\nu},$$

where

$$\beta_{\text{QCD}}/2g_s = -(\alpha_s/8\pi)b_{\text{QCD}} \quad \text{and} \quad b_{\text{QCD}} = 11 - 2n_f/3$$

and

$$\beta_{\text{QED}}/2e = -(\alpha/8\pi)b_{\text{QED}} \quad \text{and} \quad b_{\text{QED}} = -11/3.$$

Because of the anomalous coupling of the radion to gluons, the gluon fusion will be the most important production channel for the radion in hadronic collisions, followed by the WW, ZZ fusion. Figure 17 shows the production cross section of the radion at $p\bar{p}$ colliders.

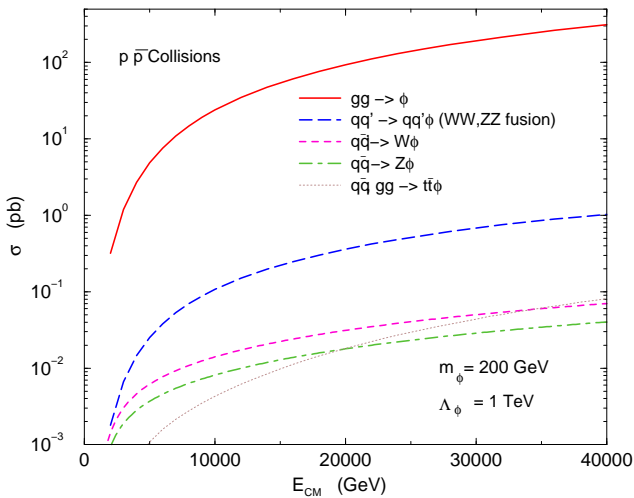


FIG. 17: Hadronic production cross sections for the radion. From Ref. [46].

One may expect that since the gluon fusion is extraordinarily large, the Tevatron dijet data might have some restriction on the radion. Figure 18 shows the 95% C.L. upper limit on the $\sigma \cdot B$, which is the cross section for a hypothetical massive particle times the branching ratio into dijet. However, the production cross section of the radion is below the CDF curve, and thus no limit is placed on the radion. Therefore, it is not desirable to detect the radion through its dijet decay mode because of the large QCD background. On the other hand, for a heavy radion the ZZ decay mode opens up and the detection is a golden mode, similar to the SM Higgs boson. Figure 19 shows the invariant mass spectrum for ZZ production. It is clear that the radion peak is very distinct above the background.

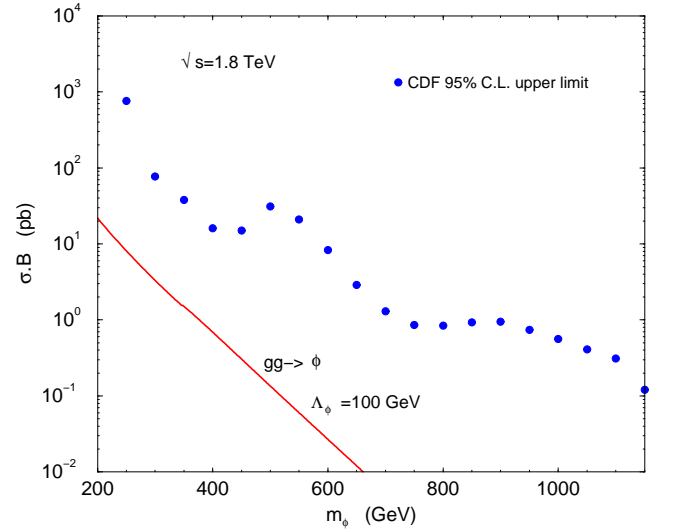


FIG. 18: 95% C.L. upper limit on $\sigma \cdot B$ for a hypothetical resonance decaying into dijet. From Ref. [46].

C. Radion-Higgs mixing

Since both the gauge and Poincare invariance do not forbid the mixing between the gravity scalar and the Higgs boson, one should expect that, in general, they should mix. The mixing term in the action is given by [44, 47]

$$S_\xi = \xi \int d^4x \sqrt{g_{\text{vis}}} R(g_{\text{vis}}) \hat{H}^\dagger \hat{H}, \quad (14)$$

where $R(g_{\text{vis}})$ is the Ricci scalar for the induced metric on the visible brane, and $\xi \rightarrow 0$ in the limit of no mixing. The free Lagrangian of the Higgs and radion is [47]

$$\begin{aligned} \mathcal{L}_0 = & -\frac{1}{2} \{1 + 6\gamma^2 \xi\} \phi_0 \square \phi_0 - \frac{1}{2} \phi_0 m_{\phi_0}^2 \phi_0 \\ & - \frac{1}{2} h_0 (\square + m_{h_0}^2) h_0 - 6\gamma \xi \phi_0 \square h_0. \end{aligned} \quad (15)$$

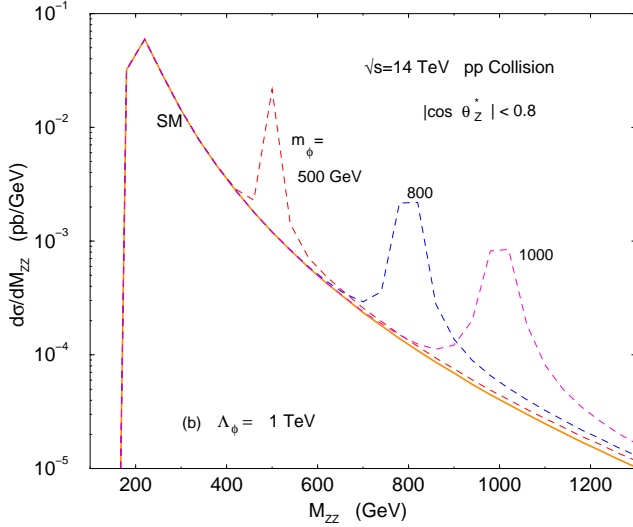


FIG. 19: The invariant mass M_{ZZ} spectrum for the radion production. From Ref. [46].

Physical states h and ϕ can be introduced to diagonalize \mathcal{L}_0 , defined by

$$\begin{pmatrix} h_0 \\ \phi_0 \end{pmatrix} = \begin{pmatrix} 1 & 6\xi\gamma/Z \\ 0 & -1/Z \end{pmatrix} \begin{pmatrix} \cos\theta & \sin\theta \\ -\sin\theta & \cos\theta \end{pmatrix} \begin{pmatrix} h \\ \phi \end{pmatrix} \quad (16)$$

$$\equiv \begin{pmatrix} d & c \\ b & a \end{pmatrix} \begin{pmatrix} h \\ \phi \end{pmatrix}, \quad (17)$$

where

$$Z^2 \equiv 1 + 6\xi\gamma^2(1 - 6\xi) \equiv \beta - 36\xi^2\gamma^2.$$

A nonzero ξ will induce some triple couplings [47, 48]

$$h-\phi-\phi, \quad h_{\mu\nu}^{(n)}-h-\phi, \quad \phi-\phi-\phi, \quad h_{\mu\nu}^{(n)}-\phi-\phi.$$

All phenomenological signatures of the RS model including the radion-Higgs mixing are specified by five parameters

$$\xi, \quad \Lambda_\phi, \quad \frac{m_0}{M_{\text{Pl}}}, \quad m_\phi, \quad m_h, \quad (18)$$

which in turns determine Λ_W and KK graviton masses $m_G^{(n)}$ as

$$\Lambda_W = \frac{\Lambda_\phi}{\sqrt{3}}, \quad m_G^{(n)} = x_n \frac{m_0}{M_{\text{Pl}}} \frac{\Lambda_W}{\sqrt{2}}. \quad (19)$$

Figure 20 shows the change in the branching ratios of the Higgs boson and the radion vs ξ . An interesting channel to probe the mixing would be the observation of the triple couplings mentioned above, e.g., in the process $e^+e^- \rightarrow G^{(n)} \rightarrow h\phi$ [48]. Figure 21 shows the cross section of this process vs ξ . It is obvious that the cross section goes to zero when $\xi \rightarrow 0$. The second part of the figure shows the region in the parameter space that can be probed in the next linear collider. A partial list of other works in radion phenomenology are listed in Refs. [49].

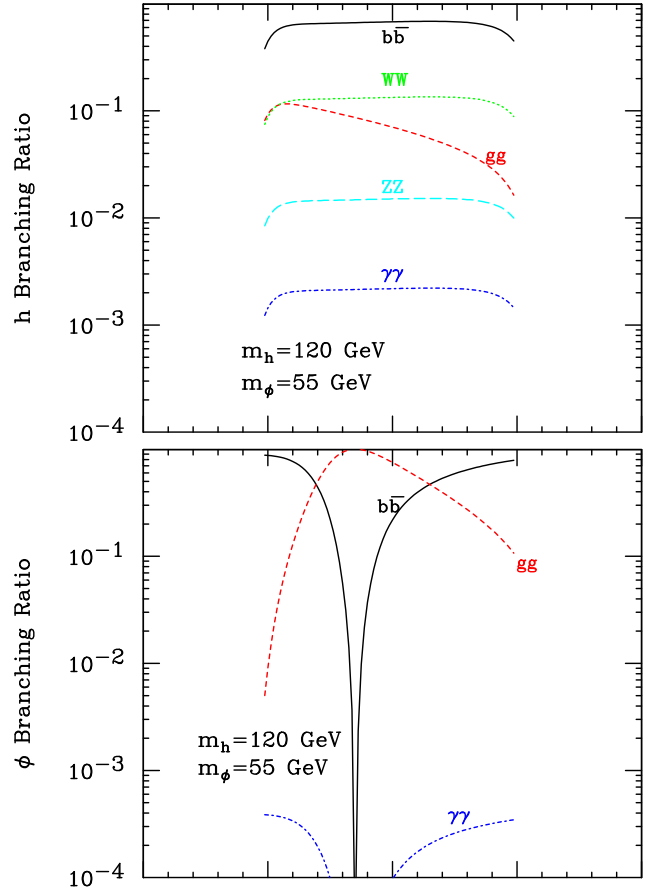


FIG. 20: The effect of the radion-Higgs mixing on the branching ratios of (a) the Higgs and (b) the radion. This is taken from Ref. [47].

IV. TeV^{-1} -SIZED EXTRA DIMENSIONS WITH GAUGE BOSONS

This scenario was originally proposed by Antoniadis [50]. Later, it was employed by Dienes et al. [51] to achieve the early gauge coupling unification. When the running scale reaches the compactification scale of the extra dimensions, the gauge couplings actually feel the strong presence of the KK states of the gauge bosons. The running of the gauge couplings will be accelerated from a logarithmic running to a power-law running. Thus, early unification is possible.

With the gauge bosons in the bulk, the KK states have masses

$$m_n^2 = m_0^2 + \sum_i^\delta \frac{n_i^2}{R^2}.$$

When the energy scale is above $\mu_0 \equiv 1/R$, the KK states contribute to physical processes, e.g., the running of the couplings:

$$\alpha_i^{-1}(\Lambda) = \alpha_i^{-1}(M_Z) - \frac{b_i}{2\pi} \ln \frac{\Lambda}{M_Z} + \frac{\tilde{b}_i}{2\pi} \ln \frac{\Lambda}{\mu_0}$$

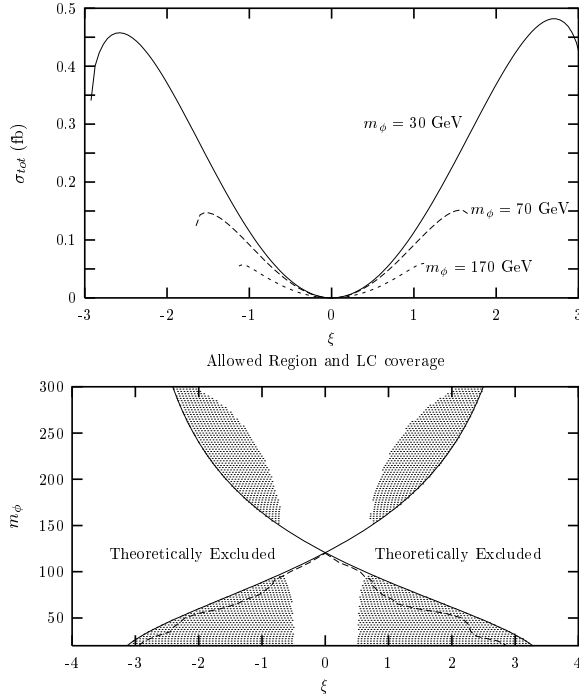


FIG. 21: The production of $e^+e^- \rightarrow G^{(n)} \rightarrow h\phi$ vs ξ , and (b) the constrained parameter space in (m_ϕ, ξ) . From Ref. [48].

$$-\frac{\tilde{b}_i X_\delta}{2\pi\delta} \left[\left(\frac{\Lambda}{\mu_0} \right)^\delta - 1 \right] \quad (20)$$

where

$$(b_1, b_2, b_3) = (33/5, 1, -3); (\tilde{b}_1, \tilde{b}_2, \tilde{b}_3) = (3/5, -3, -6);$$

$$X_\delta = \frac{2\pi^{\delta/2}}{\delta\Gamma(\delta/2)}. \quad (21)$$

Examples of early gauge coupling unification are shown in Fig. 22.

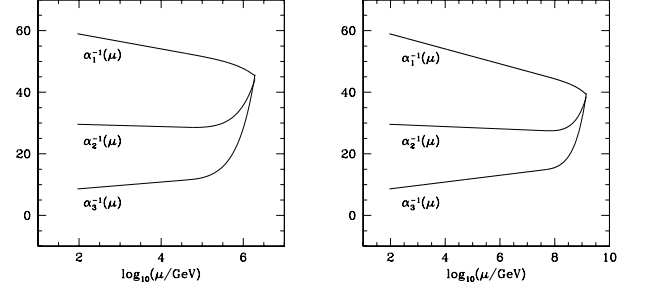


FIG. 22: Early gauge coupling unification. Here $\delta = 1$, $\mu_0 = 10^5, 10^8$ GeV, respectively. This is taken from Ref. [51].

Phenomenology of KK gauge bosons has been considered in a 5D model with the extra dimension compactified on S^1/Z_2 [52]. The 5-D Lagrangian is given by

$$\mathcal{L}_5 = -\frac{1}{4g_5} F_{MN}^2 + |D_M \phi_1|^2 + \left(i\bar{\psi} \sigma^\mu D_\mu \psi + |D_\mu \phi_2|^2 \right) \delta(x^5) \quad (22)$$

Compactifying the fifth dimension with

$$\Phi(x^\mu, x^5) = \sum_{n=0}^{\infty} \cos\left(\frac{nx^5}{R}\right) \Phi^{(n)}(x^\mu)$$

where Φ represents the gauge fields. The resulting 4-D Lagrangian becomes

$$\begin{aligned} \mathcal{L}^{\text{CC}} &= \frac{g^2 v^2}{8} \left[W_1^2 + \cos^2 \beta \sum_{n=1}^{\infty} (W_1^{(n)})^2 + 2\sqrt{2} \sin^2 \beta W_1 \sum_{n=1}^{\infty} W_1^{(n)} + 2 \sin^2 \beta \left(\sum_{n=1}^{\infty} W_1^{(n)} \right)^2 \right] \\ &+ \frac{1}{2} \sum_{n=1}^{\infty} n^2 M_c^2 (W_1^{(n)})^2 - g(W_1^\mu + \sqrt{2} \sum_{n=1}^{\infty} W_1^{(n)\mu}) J_\mu^1 + (1 \rightarrow 2) \\ \mathcal{L}^{\text{NC}} &= \frac{gv^2}{8c_\theta^2} \left[Z^2 + \cos^2 \beta \sum_{n=1}^{\infty} (Z^{(n)})^2 + 2\sqrt{2} \sin^2 \beta Z \sum_{n=1}^{\infty} Z^{(n)} + 2 \sin^2 \beta \left(\sum_{n=1}^{\infty} Z^{(n)} \right)^2 \right] \\ &+ \frac{1}{2} \sum_{n=1}^{\infty} n^2 M_c^2 \left[(Z^{(n)})^2 + (A^{(n)})^2 \right] \\ &- \frac{e}{s_\theta c_\theta} \left(Z^\mu + \sqrt{2} \sum_{n=1}^{\infty} Z^{(n)\mu} \right) J_\mu^Z - e \left(A^\mu + \sqrt{2} \sum_{n=1}^{\infty} A^{(n)\mu} \right) J_\mu^{\text{em}} \end{aligned}$$

Here we explicitly write down the charged-current (CC)

and neutral current (NC) Lagrangians.

There are two types of phenomenology associated with the KK states of the gauge bosons. First, there will be mixings with the SM W and Z bosons [53], because the KK states just have the same quantum number as the SM gauge bosons. All the weak eigenstates mix to form mass eigenstates, e.g., $Z^{(0)}$ mixes with all $Z^{(n)}$ ($n = 1 - \infty$) through a series of mixing angles; similar to $Z - Z'$ mixing. The lightest one is the Z observed at LEP. The couplings will be modified through the mixing angles. Thus, the constraints from precision measurements place limits on M_c . For example, in the presence of mixing, the Fermi constant and Z decay partial widths are modified by

$$G_F = \frac{\sqrt{2}g^2}{8M_W^2}(1 + c_\theta^2 X)(1 - 2\sin^2 \beta c_\theta^2 X)$$

$$\Gamma(Z \rightarrow f\bar{f}) = \frac{N_c M_Z}{12\pi} \frac{e^2}{s_\theta^2 c_\theta^2} (1 - 2\sin^2 \beta X)(g_v^2 + g_a^2)$$

$$X = \frac{\pi^2 M_Z^2}{3M_c^2}.$$

There have been a number of works using the electroweak precision measurements [53] to place the constraint on

$$M_c \gtrsim 3.6 \text{ TeV}.$$

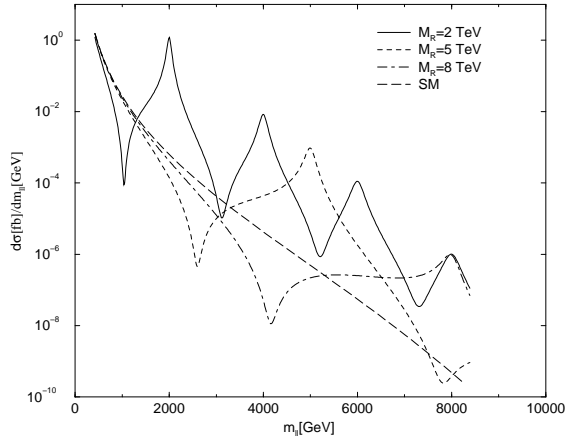


FIG. 23: The KK resonances of photon and Z in the Drell-Yan process. This is taken from Ref. [54].

On the other hand, if the energy scale is higher than the compactification scale M_c , resonances can be observed in experiments, e.g., in the Drell-Yan production [54]: see Fig. 23.

If the energy scale is smaller than M_c , we should also expect some virtual effects due to the KK states [55]. Therefore, we can use the existing high energy data to constrain the compactification scale. In the approximation

$$M_c^2 \gg \hat{s}, |\hat{t}|, |\hat{u}|,$$

the reduced amplitudes in the neutral-current scattering in $eq \rightarrow eq$ can be obtained as [55]

$$M_{\alpha\beta}^{eq}(s) = e^2 \left\{ \frac{Q_e Q_q}{s} + \frac{g_\alpha^e g_\beta^q}{\sin^2 \theta_w \cos^2 \theta_w} \frac{1}{s - M_Z^2} - \left(Q_e Q_q + \frac{g_\alpha^e g_\beta^q}{\sin^2 \theta_w \cos^2 \theta_w} \right) \frac{\pi^2}{3M_c^2} \right\}$$

where the first two terms are due to the photon and Z exchanges while the last term is due to the combined effect of the KK photons and KK Z bosons. The effects can show up in the interference terms and the pure KK term.

Cheung and Landsberg [55] used the following data sets in the analysis: (i) Drell-yan production at Tevatron, (ii) HERA NC and CC DIS, (iii) LEP II hadronic, leptonic cross section, angular distributions, (iv) dijet cross section and angular distribution, and (v) $t\bar{t}$ production. The limits obtained are shown in Table III. The overall limit is $M_c > 6.8 \text{ TeV}$, significantly improved from the electroweak precision data. We can also estimate the sensitivity reach at the Run II of the Tevatron and at the LHC [55] using the Drell-Yan process, shown in Table IV. A work by Balázs and Laforge [56] showed that using the dijet production the LHC can probe $M_c \sim 5 - 10 \text{ TeV}$.

V. UNIVERSAL EXTRA DIMENSIONS

In all previous models, all or part of the SM particles are confined to a brane while some are free to move in the extra dimensions. This kind of models is in general easier to build because we are familiar with the $3 + 1$ dimensions for a long time. However, there are no good reasons why we should confine the SM particles on a 3-brane. It is therefore appropriate to consider the scenario that all particles are free to move in all dimensions, dubbed universal extra dimensions [57]. Consider the case with only one extra dimension. The momentum conservation in the fifth dimension, after compactification, becomes conservation in KK numbers (or called KK momentum). There may be some boundary terms arising from the fixed points that break the conservation of KK numbers into a Z_2 parity, called KK parity. Odd parities are assigned to the Kaluza-Klein states with an odd KK number. Note that this breaking strength is at a few % to about 10% level compared to the SM coupling strength.

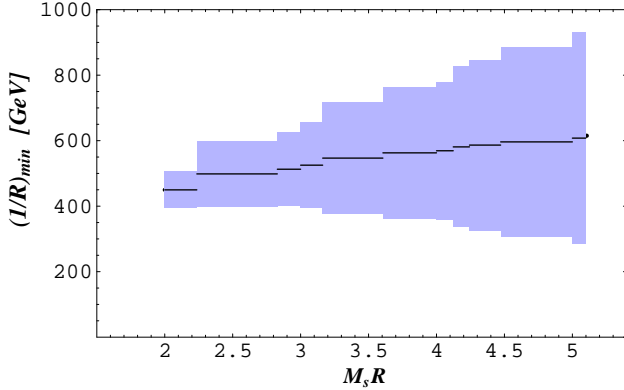
Because of the KK number conservation (the size of KK number violating couplings are much smaller) each interaction vertex involving KK states must consist of pairs of KK states of the same KK number. Therefore, in all processes the KK states must exist in pairs including internal propagators. This is in contrast to all other scenarios like ADD, bulk gauge bosons, ... Thus, the present limit on the universal extra dimension scenario is rather weak, as weak as $1/R \gtrsim 300 \text{ GeV}$ for one extra dimension [57] from precision data. For the case of two

TABLE III: Best-fit values of $\eta = \pi^2/(3M_c^2)$ and the 95% C.L. upper limits on M_c for individual data set and combinations.

	η (TeV ⁻²)	M_c^{95} (TeV)
LEP 2:		
hadronic cross section, ang. dist., $R_{b,c}$	$-0.33^{+0.13}_{-0.13}$	5.3
μ, τ cross section & ang. dist.	$0.09^{+0.18}_{-0.18}$	2.8
ee cross section & ang. dist.	$-0.62^{+0.20}_{-0.20}$	4.5
combined	$-0.28^{+0.092}_{-0.092}$	6.6
HERA:		
NC	$-2.74^{+1.49}_{-1.51}$	1.4
CC	$-0.057^{+1.28}_{-1.31}$	1.2
HERA combined	$-1.23^{+0.98}_{-0.99}$	1.6
TEVATRON:		
Drell-yan	$-0.87^{+1.12}_{-1.03}$	1.3
Tevatron dijet	$0.46^{+0.37}_{-0.58}$	1.8
Tevatron top production	$-0.53^{+0.51}_{-0.49}$	0.60
Tevatron combined	$-0.38^{+0.52}_{-0.48}$	2.3
All combined	$-0.29^{+0.090}_{-0.090}$	6.8

TABLE IV: Sensitivity reach in M_c for Run 1, Run 2 of the Tevatron and at the LHC, using the dilepton channel.

	95% C.L. lower limit on M_c (TeV)
Run 1 (120 pb ⁻¹)	1.4
Run 2a (2 fb ⁻¹)	2.9
Run 2b (15 fb ⁻¹)	4.2
LHC (14 TeV, 100 fb ⁻¹ , 3% systematics)	13.5
LHC (14 TeV, 100 fb ⁻¹ , 1% systematics)	15.5

FIG. 24: The present constraint on the universal extra dimension scenario for $\delta = 2$ and M_s is the upper cutoff. This is taken from Ref. [57].

extra dimensions the limit depends logarithmically on the cutoff scale M_s . Roughly, the limit is around 400 – 800 GeV, shown in Fig. 24.

The mass of the n th KK states is roughly n/R , where R is the compactified radius. If there were no mass splitting

among the KK states of the same n , the phenomenology would be quite boring that each $n = 1$ KK state would be stable. However, the radiative corrections and boundary terms arised lift the mass degeneracy of the states of the same n [58]. The first KK state of the hypercharge gauge boson is the lightest KK particle and it would be stable in collider experiments, and perhaps stable over cosmological time scale because of the KK parity. Figure 25 shows the spectrum and the possible decay chains of the first set of KK states after taking into account the radiative corrections [59].

Collider phenomenology is mainly the pair production of KK quarks and KK gluons [59]:

$$\begin{aligned}
qq' &\rightarrow q^{(1)}q'^{(1)} \\
q\bar{q} &\rightarrow q^{(1)}\bar{q}^{(1)} \\
gg &\rightarrow g^{(1)}g^{(1)} \\
gg, q\bar{q} &\rightarrow q'^{(1)}\bar{q}'^{(1)}
\end{aligned} \tag{23}$$

According to the decay chains shown in Fig. 25, each $q^{(1)}$ decays into jets and $\gamma^{(1)}$ eventually, thus the signature would be jets with missing energies. The signal is very similar to the weak-scale supersymmetry. A more

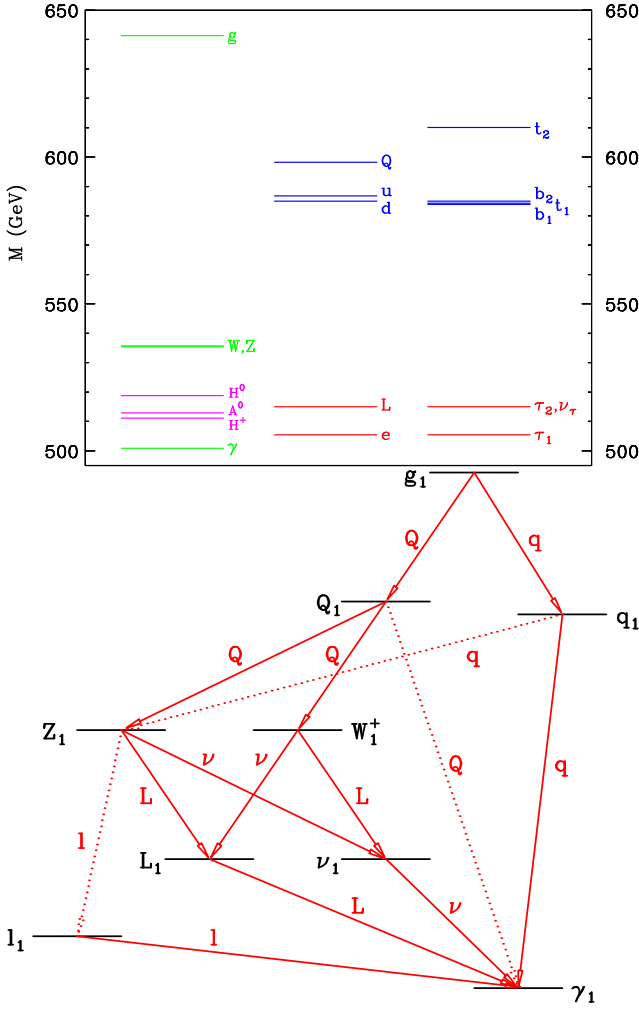


FIG. 25: The mass spectrum and the possible decay chains of the first set of KK states after taking into account the radiative corrections to the masses. These are taken from Ref. [59].

interesting decay chain would be that each $q^{(1)}$ decays into $W^{(1)}$ and $Z^{(1)}$, which in turn decay into leptons, thus giving rise to a signal of multi-leptons plus missing energies [59]. The sensitivity reach in the future collider experiments including Run II and the LHC is shown in Fig. 26. There is not much gain in the Run II of the Tevatron, but the LHC with 100 fb^{-1} integrated luminosity can probe up to $1/R \sim 1.5 \text{ TeV}$.

Yet, the most interesting feature of the universal extra dimensions is the possible candidate of the cold dark matter – the lightest KK state due to the KK parity. Servant and Tait [60] calculated the relic density with or without the coannihilation channels in Fig. 27. It is shown that for $B^{(1)}$ of order $800 - 1000 \text{ GeV}$, it forms a major component of the cold dark matter. A very striking signal of the KK dark matter is the monoenergetic positron signal [61] from the annihilation of the cold dark matter, $B^{(1)}B^{(1)} \rightarrow e^+e^-$, which can be detected at, e.g., AMS experiment. Figure 28 shows the monoenergetic positron

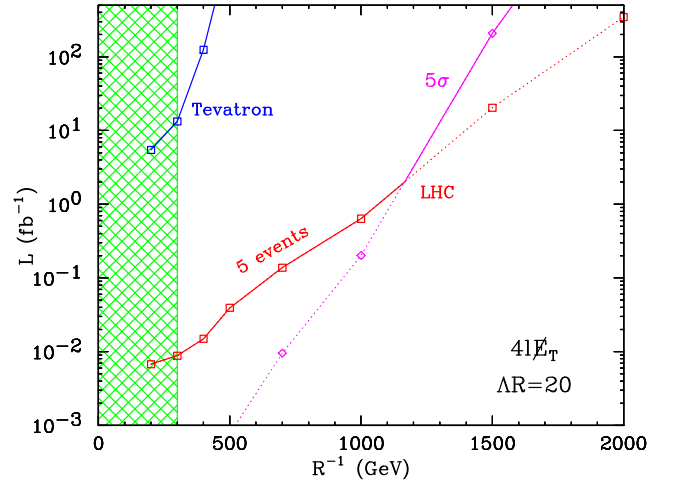


FIG. 26: Sensitivity reach on the $1/R$ scale of the universal extra dimension scenario at the RunII of the Tevatron and the LHC. This is taken from Ref. [59].

signal due to the annihilation of the KK dark matter. Since the $B^{(1)}$ pair annihilates into an electron-positron pair, the energy of the positron is monoenergetic and equal to the mass of $B^{(1)}$. This is in sharp contrast to the positron signal of other cold dark matter candidates, e.g., the lightest neutralino. However, the monoenergetic spectrum would be broadened during the propagation to the Earth, but should still be observable above the continuum background.

A partial list of other works on universal extra dimensions are listed in Refs. [62].

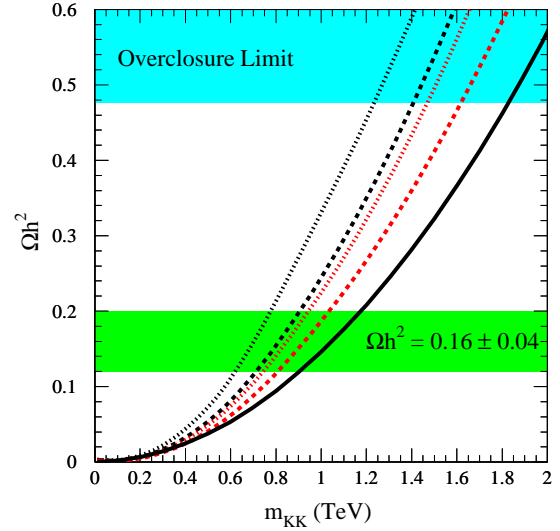


FIG. 27: The relic density Ωh^2 vs the mass of the lightest KK state $B^{(1)}$, with or without the coannihilation effects. This is taken from Ref. [60].

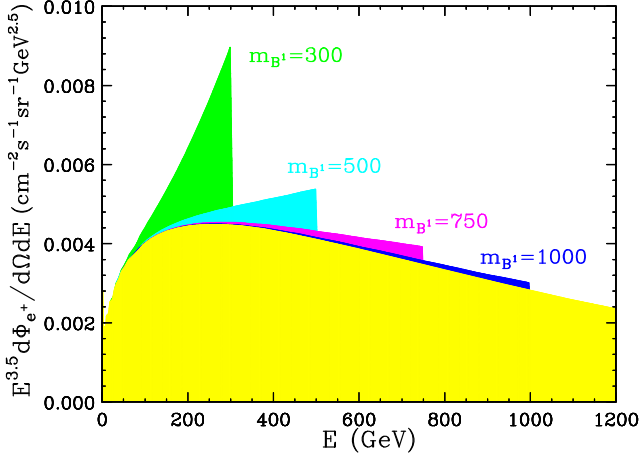


FIG. 28: The monoenergetic positron signal from the annihilation of the KK dark matter, but broadened during propagation. This is taken from Ref. [61].

VI. AN 5D SU(5) SUSY GUT MODEL

This type of grand unified models in extra dimensions is based on orbifolding. By assignment of different spatial parities (or boundary conditions) to various components of a multiplet, the component fields can have very different properties at the fixed points. Thus, it is possible to break a symmetry or to achieve the doublet-triplet splitting by the boundary conditions.

In the model by Goldberger et al. [63], they started from the Randall-Sundrum scenario [40]: a slice of AdS space with two branes (the Planck brane and the TeV brane), one at each end. The hierarchy of scales is generated by the AdS warp factor k , which is of order of the five-dimensional Planck scale M_5 , such that the 4D Planck scale is given by $M_{\text{Pl}}^2 \sim M_5^3/k$. The fundamental scale on the Planck brane is M_{Pl} while the fundamental scale on the TeV brane is rescaled to TeV by the warp factor: $T \equiv ke^{-\pi k R}$, where R is the size of the extra dimension. The setup is shown in Fig. 29. The model is an 5D supersymmetric SU(5) gauge theory compactified on the orbifold S^1/Z_2 in the AdS space. The boundary conditions break the SU(5) symmetry and provide a natural mechanism for the Higgs doublet-triplet splitting and suppress the proton decay [64]. The Planck brane respects the SM gauge symmetry while the TeV brane respects the SU(5) symmetry. The matter fermions reside on the Planck brane. By the boundary conditions the wave-functions of the color-triplet Higgs fields are automatically zero at the Planck brane, on which the matter fermions reside, while the doublet Higgs fields are nonzero at the Planck brane and give Yukawa couplings to the matter fermions. Thus, the excessive proton decay via the color-triplet Higgs fields is highly suppressed, and the doublet-triplet splitting is therefore natural by the boundary conditions. The mass of the color-triplet

fields (and the XY gauge bosons) is given by the warp factor and is of a TeV scale, the same as the KK states of other fields in the setup.

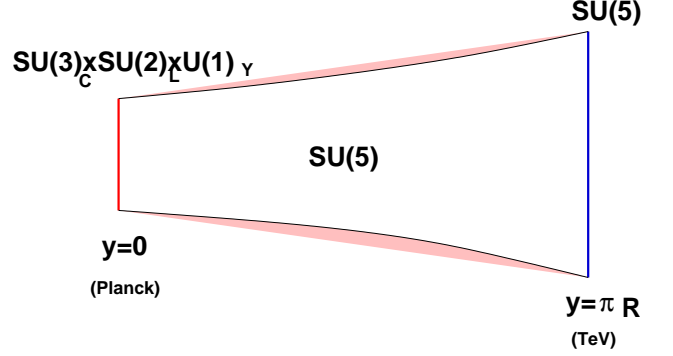


FIG. 29: A model of 5D SU(5) SUSY GUT on a slice of AdS space, due to Goldberger, Nomura, and Smith [63].

The striking signature of this type of GUT models is the TeV colored Higgs bosons [65], in contrast to the conventional proton decay signature. Such TeV colored Higgs bosons can be copiously produced at the upcoming LHC. Since these colored Higgs bosons do not couple to matter fermions or weak gauge bosons, they couple only to the gluons. The interaction is described by

$$\mathcal{L} = -ig_s H_C^* \overleftrightarrow{\partial}_\mu H_C T^a A^{a\mu} + g_s^2 T^a T^b H_C^* H_C A_\mu^a A^{b\mu}. \quad (24)$$

Production is via the $q\bar{q}$ and gg fusion. The cross section formulas can be found in Ref. [65]. The total production cross section is illustrated in Fig. 30.

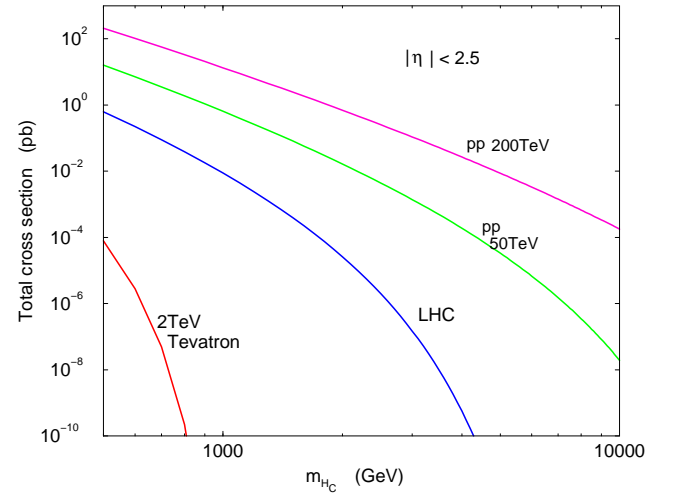


FIG. 30: Total production cross section for the colored Higgs bosons in pp collisions. From Ref. [65].

The detection of the colored Higgs boson depends on its decay modes. From Eq. (24) it is clear that the colored Higgs boson must be coupled pairwise to gluons and so itself cannot decay into gluons. However, the colored

Higgs boson will couple to its own supersymmetric partner, the colored Higgsino, and the gluino or gravitino. In general, we expect the masses of the colored Higgs boson and the colored Higgsino to be of the same order. Here we assume that the mass of the colored Higgs boson is less than the sum of the masses of the colored Higgsino and the gluino (or the gravitino), such that the colored Higgs boson is stable at least within the detector.

Once the colored Higgs bosons are produced, they will hadronize into massive stable particles, electrically either neutral or charged. For both neutral or charged states, they will undergo very little hadronic energy loss in the detector, because of the very small momentum transfer between the Higgs boson and the detector material. Therefore, the neutral state will escape detection unnoticed. The charged state will also undergo the ionization energy loss though, through which it is detected. The ionization energy loss dE/dx is very standard and can be found in Particle Data Book. The dE/dx almost has no explicit dependence on the mass of the particle. The dependence comes in through the factor $\beta\gamma \equiv p/M$, in particular for the range $0.1 < \beta\gamma < 1$, dE/dx is almost a linear function of $\beta\gamma$ and has no dependence on the mass. Therefore, by measuring dE/dx the p/M can be deduced. If the momentum p is measured simultaneously, the mass M of the particle can be estimated.

Experimentally, the massive stable charged particle will produce a track in the central tracking and/or silicon vertex system, where dE/dx and p can be measured, provided that $\beta\gamma$ is not too large ($\beta\gamma < 0.85$). In the current search for stable charged particles, the CDF Collaboration also required the particle to penetrate to the outer muon chamber. This is possible if the initial $(\beta\gamma)_0 \gtrsim 0.25 - 0.5$. Therefore, we can call the signature the “heavy muon”. We have verified that for a 1 TeV particle the requirement on $(\beta\gamma)_0$ is similar.

The event rate can be estimated including the following factors:

- The probability $P = 1/2$ for the colored Higgs boson to hadronize into a charged state.
- Require at least one colored Higgs boson to be in the detection range: $0.25 < \beta\gamma < 0.85$ and $|\eta| < 2.5$.
- An efficiency factor of 80% for seeing a track in the central tracking chamber.

Note that the $\beta\gamma \equiv p/M > 0.25$ cut means $p > 250$ GeV for a 1 TeV particle, which makes it background free from μ^\pm, K^\pm, π^\pm . The event rates are shown in Table V. The RunII with a 20 fb^{-1} is sensitive to a mass of about 400 GeV. The LHC is sensitive up to about 1.5 TeV [65].

VII. CONCLUSIONS

There should not be any conclusions as this area is growing so fast that interesting scenarios are popping up all the times. We have to keep our eyes open for viable models.

So far, there have been extensive studies of sub-Planckian and trans-Planckian collider signatures for the large extra dimension model (ADD model). Experimentally, there are already some limits around $M_D \sim 1 - 1.4$ TeV for the fundamental Planck scale.

The most striking feature of the Randall-Sundrum model is that it has a distinct unevenly spaced KK spectrum. However, the first sign at colliders is perhaps the radion or radion-Higgs mixing effects.

The TeV^{-1} -sized extra dimensions with gauge bosons will modify the gauge coupling running, and affect the precision measurements, and high energy scattering processes. The current best limit is about $M_c > 6.8$ TeV. On the other hand, the scenario with every particle in the extra dimensions (universal extra dimensions) has a very different phenomenology. The presence of KK number conservation renders that the KK particles must be produced in pairs even in loop level. Therefore, the present limit is rather weak, of order of $300 - 800$ GeV from precision measurements. The lightest KK state is stable over cosmological time scale and could be a dark matter candidate if it has a mass around $800 - 1000$ GeV.

Finally, I have also mentioned an 5D SU(5) SUSY GUT model in AdS space, which can have safe proton decay, a natural doublet-triplet splitting, and a TeV colored Higgs triplet. The TeV colored Higgs boson becomes an alternative signature for this kind of GUT, in contrast to proton decay. The TeV colored Higgs boson can be copiously produced at hadronic colliders, e.g. the LHC, and gives an interesting “heavy muon”-like signature. The LHC is sensitive up to about 1.5 TeV.

I have benefitted a lot from other recent reviews [66, 67, 68, 69, 70, 71] on these subjects.

Acknowledgments

I would like to thank DØ Collaboration, Feng, Shapere, Hewett, Spiropulu, Davoudiasl, Rizzo, Dominici, Grzadkowski, Gunion, Toharia, Dienes, Dudas, Gherghetta, Nath, Yamada, Yamaguchi, Appelquist, Cheng, Dobrescu, Matchev, Schmaltz, Servant, and Tait for using their figures in this talk and report. I would also like to thank Wai-Yee Keung, Greg Landsberg, Chung-Hsien Chou, C.S. Kim, Jeonghyeon Song, and Gi-Chol Cho for collaborations on various parts of this talk and report.

[1] The LEP Collaborations Electroweak Working Group, LEPEWWG/2002-01.

[2] CDF Coll., Phys. Rev. Lett. **74**, 2626 (1995); DØ Coll.

TABLE V: Event rates for the production of colored Higgs bosons at the Tevatron, the LHC and the future pp colliders of 50 and 200 TeV.

m_{HC} (TeV)	Tevatron ($\mathcal{L} = 20 \text{ fb}^{-1}$)	LHC ($\mathcal{L} = 100 \text{ fb}^{-1}$)	VLHC 50 TeV ($\mathcal{L} = 100 \text{ fb}^{-1}$)	VLHC 200 TeV ($\mathcal{L} = 100 \text{ fb}^{-1}$)
0.3	160	2.3×10^5	3.1×10^6	2.8×10^7
0.4	14	5.5×10^4	9.6×10^5	9.7×10^6
0.5	0.9	1.7×10^4	3.7×10^5	4.3×10^6
0.8	-	1200	4.7×10^4	7.1×10^5
1.0	-	285	1.6×10^4	2.9×10^5
1.5	-	15	2200	5.6×10^4
2.0	-	1.2	470	1.6×10^4
3.0	-	-	43	2700
4.0	-	-	6.4	690
6.0	-	-	-	90
8.0	-	-	-	19
9.0	-	-	-	9.7

- Phys. Rev. Lett. **74**, 2632 (1995).
- [3] N. Arkani-Hamed, S. Dimopoulos, and G. Dvali, Phys. Lett. **B429**, 263 (1998); I. Antoniadis, N. Arkani-Hamed, S. Dimopoulos, and G. Dvali, Phys. Lett. **B436**, 257 (1998); N. Arkani-Hamed, S. Dimopoulos, and G. Dvali, Phys. Rev. **D59**, 086004 (1999).
- [4] G. Giudice, R. Rattazzi, and J. Wells, Nucl. Phys. **B544**, 3 (1999) and revised version 2, e-print hep-ph/9811291.
- [5] T. Han, J.D. Lykken, and R.-J. Zhang, Phys. Rev. D **59**, 105006 (1999) and revised version 4, e-print hep-ph/9811350.
- [6] E.A. Mirabelli, M. Perelstein, and M.E. Peskin, Phys. Rev. Lett. **82**, 2236 (1999).
- [7] J.L. Hewett, Phys. Rev. Lett. **82**, 4765 (1999).
- [8] S. Nussinov and R. Shrock, Phys. Rev. D **59**, 105002 (1999).
- [9] T. Rizzo, Phys. Rev. D **59**, 115010 (1999).
- [10] K. Cheung and W.-Y. Keung, Phys. Rev. **D60**, 112003 (1999).
- [11] C. Balázs et al., Phys. Rev. Lett. **83**, 2112 (1999).
- [12] CDF Coll. Phys. Rev. Lett. **89**, 281801 (2002).
- [13] DØ Coll., hep-ex/0302014.
- [14] K. Cheung, Phys. Lett. **B460**, 383 (1999).
- [15] K. Cheung and G. Landsberg, Phys. Rev. **D62**, 076003 (2000).
- [16] K. Cheung, Phys. Rev. **D61**, 015005 (2000).
- [17] O.J.P. Éboli et al., Phys. Rev. **D61**, 094007 (2000).
- [18] G. Shiu, R. Shrock, and S. Tye, Phys. Lett. **B458**, 274 (1999).
- [19] D. Bourilkov, JHEP **9908**, 006 (1999).
- [20] K. Agashe and N. Deshpande, Phys. Lett. **B456**, 60 (1999).
- [21] D. Atwood, S. Bar-Shalom, and A. Soni, Phys. Rev. **D61**, 054003 (2000).
- [22] K. Lee, H. Song, and J. Song, Phys. Lett. **B464**, 82 (1999).
- [23] P. Mathews, S. Raychaudhuri, and K. Sridhar, JHEP **0007**, 008 (2000).
- [24] P. Mathews, S. Raychaudhuri, and K. Sridhar, Phys. Lett. **B450**, 343 (1999).
- [25] M. Graesser, Phys. Rev. **D61**, 074019 (2000).
- [26] DØ Coll. Phys. Rev. Lett. **86**, 1156 (2001).
- [27] P. Argyres, S. Dimopoulos, and J. March-Russell, Phys. Lett. **B441**, 96 (1998).
- [28] S. Giddings and S. Thomas, Phys. Rev. **D65**, 056010 (2002).
- [29] S. Dimopoulos and G. Landsberg, Phys. Rev. Lett. **87**, 161602 (2001).
- [30] S. Dimopoulos and R. Emparan, Phys. Lett. **B526**, 393 (2002).
- [31] R. Myers and M. Perry, Ann. Phys. **172**, 304 (1986).
- [32] S.B. Giddings, hep-ph/0110127.
- [33] K. Cheung, Phys. Rev. Lett. **88**, 221602 (2002).
- [34] R. Emparan, G. Horowitz, and R. Myers, Phys. Rev. Lett. **85**, 499 (2000).
- [35] R. Casadio and B. Harms, Phys. Lett. **B487**, 209 (2000); Phys. Rev. **D64**, 024016 (2001); V. Frolov and D. Stojkovic, Phys. Rev. **D66**, 084002 (2002); Phys. Rev. Lett. **89**, 151302 (2002).
- [36] K. Cheung, Phys. Rev. **D66**, 036007 (2002).
- [37] E. Ahn, M. Cavaglia, and A. Olinto, Phys. Lett. **B551**, 1 (2003).
- [38] J. Feng and A. Shapere, Phys. Rev. Lett. **88**, 021303 (2002).
- [39] S. Hossenfelder, S. Hofmann, M. Bleicher, and H. Stöcker, hep-ph/0109085; R. Casadio and B. Harms, hep-th/0110255; S. Hofmann et al., hep-ph/0111052; S. Park and H. Song, hep-ph/0111069; G. Landsberg, Phys. Rev. Lett. **88**, 181801 (2002); G. Giudice, R. Rattazzi and J. Wells, Nucl. Phys. **B630**, 293 (2002); M. Bleicher et al., hep-ph/0112186; S. Solodukhin, Phys. Lett. **B533**, 153 (2002); T. Rizzo, JHEP **0202**, 011 (2002); K. Cheung and C.-H. Chou, Phys. Rev. **D66**, 036008 (2002). L. Anchordoqui, H. Goldberg, and A. Shapere, hep-ph/0204228; P. Jain, D. McKay, S. Panda, and J. Ralston, Phys. Lett. **B484**, 267 (2000); L. Anchordoqui, J. Feng, H. Goldberg, and A. Shapere, Phys. Rev. **D65**, 124027 (2002); L. Anchordoqui and H. Goldberg, Phys. Rev. **D65**, 047502 (2002); R. Emparan, M. Masip, and R. Rattazzi, Phys. Rev. **D65**, 064023 (2002); A. Ring-

- wald and H. Tu, Phys. Lett. **B525**, 135 (2002); Y. Uehara, Prog. Theor. Phys. **107**, 621 (2002); M. Kowalski, A. Ringwald, and H. Tu, Phys. Lett. **B529**, 1 (2002); J. Alvarez-Muniz, J. Feng, F. Halzen, T. Han, and D. Hooper, Phys. Rev. **D65**, 124015 (2002).
- [40] L. Randall and R. Sundrum, Phys. Rev. Lett. **83**, 3370 (1999); *ibid.* **83**, 4690 (1999).
- [41] H. Davoudiasl, J. Hewett, and T. Rizzo, Phys. Rev. Lett. **84**, 2080 (2000).
- [42] W. Goldberger and M. Wise, Phys. Rev. Lett. **83**, 4922 (1999).
- [43] C. Csáki, M. Graesser, L. Randall, and J. Terning, Phys. Rev. **D62**, 045015 (2000).
- [44] G. Giudice, R. Rattazzi and J. Wells, Nucl. Phys. **B595**, 250 (2001).
- [45] H. Davoudiasl, J. Hewett, and T. Rizzo, Phys. Rev. **D63**, 075004 (2001).
- [46] K. Cheung, Phys. Rev. **D63**, 056007 (2001).
- [47] D. Dominici, B. Grzadkowski, J. Gunion, and M. Toharia, hep-ph/0206192.
- [48] K. Cheung, C. Kim, and J. Song, hep-ph/0301002.
- [49] W. Goldberger and M. Wise, Phys. Lett. **B475**, 275 (2000); S. Bae, P. Ko, H. Lee and J. Lee, Phys. Lett. **B487**, 299 (2000). C. Csaki, M. Graesser and G. Kribs, Phys. Rev. **D63**, 065002 (2001); C. Kim, J. Kim, and J. Song, Phys. Lett. **B511**, 251 (2001); C. Kim, J. Kim, and J. Song, hep-ph/0204002; U. Mahanta and S. Rakshi, Phys. Lett. **B480**, 176 (2000); U. Mahanta and A. Datta, Phys. Lett. **B483**, 196 (2000); S. Park, H. Song and J. Song, Phys. Rev. **D65**, 075008 (2002); S. Park, H. Song and J. Song, Phys. Rev. **D63**, 077701 (2001); C. Kim, K. Lee, and J. Song, Phys. Rev. **D64**, 015009 (2001); M. Chaichian, A. Datta, K. Huitu and Z. Yu, Phys. Lett. **B524**, 161 (2002); T. Han, G. Kribs, and B. McElrath, Phys. Rev. **D64**, 076003 (2001); J. Hewett and T. Rizzo, hep-ph/0202155.
- [50] I. Antoniadis, Phys. Lett. **B246**, 377 (1990).
- [51] K. Dienes, E. Dudas, and T. Gherghetta, Phys. Lett. **B436**, 55 (1998); Nucl. Phys. **B537**, 47 (1999).
- [52] A. Pomarol and M. Quirós, Phys. Lett. **B438**, 255 (1998); M. Masip and A. Pomarol, Phys. Rev. **D 60**, 096005 (1999); I. Antoniadis, K. Benakli, and M. Quirós, Phys. Lett. **B460**, 176 (1999).
- [53] P. Nath and M. Yamaguchi, Phys. Rev. **D60**, 116004 (1999); R. Casalbuoni, S. Curtis, D. Dominici, and R. Gatto, Phys. Lett. **B462**, 48 (1999); A. Strumia, Phys. Lett. **B466**, 107 (1999); C. Carone, Phys. Rev. **D61**, 015008 (2000); T. Rizzo and J. Wells, Phys. Rev. **D61**, 016007 (2000); A. Delgado, A. Pomarol, and M. Quirós, JHEP **0001**, 030 (2000); F. Cornet, M. Relaño, and J. Rico, Phys. Rev. **D61**, 037701 (2000); A. Mück, A. Pilaftsis, and R. Rückl, Phys. Rev. **D65**, 085037 (2002).
- [54] P. Nath, Y. Yamada, and M. Yamaguchi, Phys. Lett. **B466**, 100 (1999); I. Antoniadis, K. Benakli, and M. Quiros, Phys. Lett. **B331**, 313 (1994).
- [55] K. Cheung and G. Landsberg, Phys. Rev. **D65**, 076003 (2002).
- [56] C. Balázs and B. Laforge, Phys. Lett. **B525**, 219 (2002).
- [57] T. Appelquist, H. Cheng, and B. Dobrescu, Phys. Rev. **D64**, 035002 (2001).
- [58] H. Cheng, K. Matchev, and M. Schmaltz, Phys. Rev. **D66**, 036005 (2002).
- [59] H. Cheng, K. Matchev, and M. Schmaltz, Phys. Rev. **D66**, 056006 (2002).
- [60] G. Servant and T. Tait, Nucl. Phys. **B650**, 391 (2003).
- [61] H. Cheng, J. Feng, and K. Matchev, Phys. Rev. Lett. **89**, 211301 (2002).
- [62] K. Agashe, N. Deshpande, and G. Wu, Phys. Lett. **B514**, 309 (2001); T. Appelquist and B. Dobrescu, Phys. Lett. **B516**, 85 (2001); T. Rizzo, Phys. Rev. **D64**, 095010 (2001); C. Macesanu, C. McMullen, and S. Nandi, Phys. Rev. **D66**, 015009 (2002); F. Petriello, JHEP **0205**, 003 (2002); C. Macesanu, C. McMullen, and S. Nandi, Phys. Lett. **B546**, 253 (2002); T. Appelquist and H. Yee, Phys. Rev. **D67**, 055002 (2003); D. Chakraverty, K. Huitu, and A. Kundu, Phys. Lett. **B558**, 173 (2003); J. Oliver, J. Papavassiliou, and A. Santamaria, Phys. Rev. **D67**, 056002 (2003); A. Buras, M. Spranger, and A. Weiler, hep-ph/0212143; R. Mohapatra and A. Perez-Lorenzana, hep-ph/0212254.
- [63] W. Goldberger, Y. Nomura, and D. Smith, hep-ph/0209158; see also earlier works by A. Pomarol, Phys. Rev. Lett. **85**, 4004 (2000); T. Gherghetta and A. Pomarol, Nucl. Phys. **B602**, 3 (2001).
- [64] Y. Kawamura, Prog. Theor. Phys. **105**, 999 (2001).
- [65] K. Cheung and G.-C. Cho, Phys. Rev. **D67**, 075003 (2003).
- [66] J. Hewett and M. Spiropulu, hep-ph/0205106.
- [67] A review by J. Hewett and J. March-Russell in PDB, H. Hagiwara et al. (Particle Data Group), Phys. Rev. **D66**, 010001 (2002).
- [68] K. Kisselev, hep-ph/0303090.
- [69] G. Landsberg, hep-ex/0105039.
- [70] K. Cheung, hep-ph/0003306.
- [71] K. Sridhar, Int. J. Mod. Phys. **A15**, 2397 (2000).